Nanoscale

Accepted Manuscript

This article can be cited before page numbers have been issued, to do this please use: X. Yang, N. Wang, L. Zhang, L. Dai, H. Shao and X. Jiang, *Nanoscale*, 2017, DOI: 10.1039/C7NR00342K.

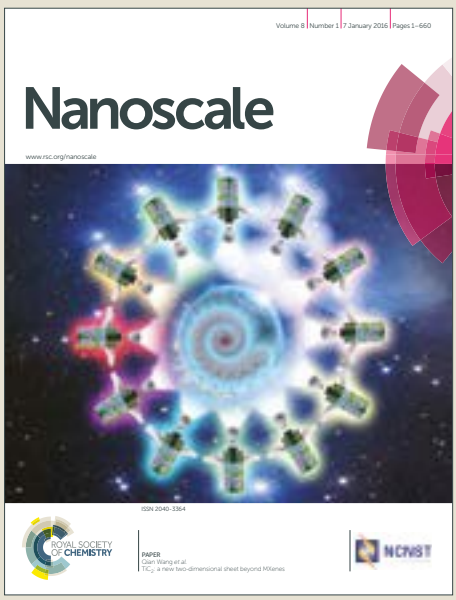

ROYAL SOCIETY OF CHEMISTRY

rsc.li/nanoscale

View Article Online
DOI: 10.1039/C7NR00342K

Journal Name

ARTICLE

Organic nanostructure-based probes for two-photon imaging of mitochondria and microbes with emission between 430 nm and 640 nm

Received 00th January 20xx,
Accepted 00th January 20xx

DOI: 10.1039/x0xx00000x

www.rsc.org/

Xinglong Yang[a,b,c], Nuoxin Wang[b], Lingmin Zhang[b], Luru Dai[b], Huawu Shao[a,*], and Xingyu Jiang[b,*]

Multi-photon excitation and versatile fluorescent probes are in high need for biological imaging, since one probe can satisfy many needs as biosensor. Herein we synthesize a series of two-photon excited probes based on tetraphenylethene (TPE) structures (TPE-Acr, TPE-Py, and TPE-Quino), which can image both mammalian cells and bacteria based on aggregation-induced emission (AIE) without washing them. Because of cationic moieties, the fluorescent molecules can aggregate into nanoscale fluorescent organic nanoscale dots to image mitochondria and bacteria with tunable emissions using both one-photon and two-photon excitation. Our research demonstrates that these AIE-dots expand the functions of luminescent organic dots to construct efficient fluorescent sensor applicable to both one-photon and two-photon excitation for bio-imaging of bacteria and mammalian cells.

Introduction

Mitochondria, as power house of eukaryotic cells, play a paramount role in converting oxygen and nutrients into adenosine triphosphate (ATP) which powers the cellular metabolic activities. Many types of human diseases appear when mitochondrial dysfunction appears, such as myopathy, diabetes, cardiovascular disorders and so on.[1-4] Mitochondrial targeting and imaging are important for biological and medical sciences.[5, 6] The design of multi-color and high signal-to-noise fluorescent probes for the mitochondria has become critical for biologists and chemists alike.

Researchers have developed various fluorescent organic molecular nanostructure probes in recent years.[7-10] With the extraordinary development of aggregation-induced emission (AIE) fluorogens, scientists use many AIE probes to image living cells and organs based on their good photostability and high signal-noise ratio.[11] The AIE probes show high emission with the aggregation of molecules, and the aggregation in the solution can form nanoscale structures, which is called AIE-dots comprising AIE organic molecules. The AIE dots are good candidates for biosensing and bioimaging on the basis of the better optical properties and biocompatibility compared with traditional small organic fluorophores.[12]

Some AIE probes can target certain subcellular organelles, such as the mitochondria and lysosome.[13, 14] Researchers have reported a mitochondrial targeting AIE luminogen.[15] We apply tetraphenylethene-indolium molecule (TPE-indo) to target mitochondria in the living cells successfully.[16] TPE-indo is a red-emission mitochondrial probe, and can monitor the change of mitochondrial membrane potential, which shows different bioimaging behavior compared with the other reported AIE probes.

Bacteria, as the ancestor of mitochondria according to the viewpoints of the endosymbiosis hypothesis, exhibit similar electrophysiological behavior with the inner mitochondrial membrane.[17, 18] Microbes and fungi are negatively charged due to the presence of polysaccharides within the wall and cell membrane macromolecules which contain phosphates, proteins, and carboxylate groups.[19] Bacteria give rise to infections which causes significant mortality and morbidity worldwide.[20] Examples of bacteria that trigger serious infections include *Streptococcus*, *Staphylococcus,* and *Escherichia coli* (*E. coli*). Many types of fungi can also be pathogenic. For example, *Candida albicans* (*C. albicans*) are an opportunistic pathogen and they can wreak havoc on our immune system when their toxic byproducts diffuse and spread.[21] So the imaging, detection, and eradication of bacteria are necessary. Our group has developed antibacterial nanomaterials, such as small molecule-modified gold nanoparticles and bimetallic nanoparticles.[22-25] Certain molecules with AIE can also bind with bacteria and show bright emission. For instance, we also make use of AIE probes to distinguish eight types of bacteria.[26] These results suggest that AIE probes can image mitochondria and bacteria simultaneously. Because most of the fluorescent probes have one-photon excitations and short emission wavelengths such that autofluorescence of biological samples and photo-damage to living

[a] *Natural Products Research Center, Chengdu Institute of Biology, Chinese Academy of Sciences, Chengdu, Sichuan, 610041, China.*
[b] *CAS Center for Excellence in Nanoscience, CAS Key Lab for Biological Effects of Nanomaterials and Nanosafety, National Center for NanoScience and Technology, ZhongGuanCun BeiYiTiao, Beijing, 100190, China.*
[c] *University of Chinese Academy of Science, Beijing, 100049, China.*
**Corresponding authors: Huawu Shao, Email: shaohw@cib.ac.cn, Tel.: +86-028-82890818; Xingyu Jiang, Email: xingyujiang@nanoctr.cn, Tel.: +86-10-82545558.*
Electronic Supplementary Information (ESI) available: Figures S1 through S3. See DOI: 10.1039/x0xx00000x

View Article Online
DOI: 10.1039/C7NR00342K

organisms are inevitable.[27] Two-photon fluorescent (TPFL) probes have recently shown promise in overcoming these drawbacks of probes that rely on one-photon excitation. For example, TPFL probes undergo low photobleaching, have deep tissue penetration capability, low background signal and low phototoxicity via the use of near infrared excitation.[28] The two-proton absorbing chromophores in TPFL probes contain similar molecular geometry, such as D-π-A (donor group-π-conjugated group-acceptor group), A-π-A or D-π-D geometry.[29-32] Organic nanoscale probes, such as AIE-dots are mostly prominent with two-proton fluorescence.[33, 34] If we construct a probe with AIE group as a donor, another mitochondrial targeting group as an acceptor and a π bond as a linkage, we may obtain a tetraphenylethene (TPE) [35] probe with AIE and TPFL properties. Here we show that when we change the acceptor, we can tune the emission spectra of the molecules, and illustrate a series of TPE-based nano probes in a broad emission range.

Here, we develop tunable one/two-photon fluorescent probes based on organic molecular nanostructures with TPE, and apply them in sensing and imaging both mitochondria and bacteria because of their presumed similar evolutionary origin. On the basis of the reported results, in most cases the mitochondrial probes can also enter bacteria.[36, 37] The inner membrane of cellular mitochondria is similar to bacterial membrane which has negative charges.[38, 39] We design and synthesize a series of TPE-based nitrogen (N)-containing heterocycles by coupling pyridine (Py), quinoline (Quino) or acridine (Acr) salts with TPE. Py, Quino, and Acr have different amounts of phenyl groups and when they couple with TPE, the new fluorogens may have different emissions.[40, 41] We apply TPE as a chromophore and an electron donor with AIE ability, while Py, Quino, and Acr are the functional groups of imaging mitochondria and electron accepters which have positive charge. A π bond links the electron donor and electron acceptor, thus construct a D-π-A geometry. Py, Quino, and Acr have N-positive charges, which can facilitate binding with the mitochondria and bacteria. Moreover, the three functional groups have similar structures to some degree, while they have different stereochemistry. We plan to apply the difference of these molecular structures to endow the probes with tunable emission and one/two-proton fluorescence, and carry out bioimaging in cells and microbes.

Materials and methods

Materials

2-methylpyridine, 4-methylquinoline, and iodomethane are from Aldrich. 9-methylacridine is from Heowns in china and we use it without further purification. Other reagents are all of analytical reagent grade. We use a Milli-Q purification system to obtain pure water (18.2 MΩ˙cm).

Instrumentation

We use a Bruker ARX 400 NMR spectrometer to yield the ^{1}H and ^{13}C NMR spectra. We utilize a UV-2450 Shimadzu spectrophotometer at room temperature to produce the absorption spectra. We employ a Perkin-Elmer LS55 luminescence spectrometer to obtain the fluorescence spectrum. A Tecnai G2 20 S-TWIN transmission electron microscope operating at an acceleration voltage of 200 kV gives us the TEM images.

Synthesis

Synthesis of 1,2-dimethylpyridinium iodide[42] We add 2-methylpyridine (186 mg, 2 mmol) and methyl iodide (853 mg, 6 mmol) in acetone (10 mL) and then reflux the mixture for 2 h. We filter off the precipitated crystals and dry them under vacuum. We obtain the product as white solid (330 mg, yield: 71%). 1H NMR (400 MHz, DMSO) δ 9.01 (d, J = 6.2 Hz, 1H), 8.49 (td, J = 7.9, 0.8 Hz, 1H), 8.07 (d, J = 7.9 Hz, 1H), 7.96 (t, J = 6.9 Hz, 1H), 4.26 (s, 3H), 2.81 (s, 3H).

1,4-dimethylquinolinium iodide[43] We dissolve 4-methylquinoline (250 mg, 1.75 mmol) in benzene (25 mL). We add an excess of methyl iodide (853 mg, 6 mmol) at room temperature. Then the mix solution is refluxed for 1 h. After the mixture cools down to room temperature, we filter the precipitate, wash with benzene, dry it to obtain a yellow solid (474 mg, yield: 95%). 1H NMR (400 MHz, DMSO) δ 9.38 (d, J = 6.0 Hz, 1H), 8.58 – 8.46 (m, 2H), 8.28 (ddd, J = 8.7, 7.0, 1.3 Hz, 1H), 8.08 (dd, J = 10.9, 3.5 Hz, 2H), 4.59 (s, 3H), 3.01 (s, 3H).

9,10-dimethylacridinium iodide We add methyl iodide (2.1 g, 15 mmol) to the mixture solution of 9-methylacridine (0.14 g, 0.14 mmol) in dry tetrahydrofuran and acetonitrile under a nitrogen atmosphere. We keep the temperature of the solution at 40 ^{o}C for 24 h under nitrogen atmosphere in the dark. We filter and recrystallize the precipitate in methanol-anhydrous ether and dry to obtain a red solid (0.21 g, yield: 45%). 1H NMR (400 MHz, DMSO) δ 8.93 (d, J = 8.6 Hz, 2H), 8.77 (d, J = 9.1 Hz, 2H), 8.43 (t, J = 7.7 Hz, 2H), 8.03 (t, J = 7.5 Hz, 2H), 4.82 (s, 3H), 3.53 (s, 3H).

4-(1,2,2-triphenylvinyl)benzaldehyde (TPE-CHO) To a solution of bromotripphenylethylene (1.68 g, 5 mmol) and 4-formylphenylboronic acid (1.13 g, 7.5 mmol) in toluene (30 mL), we add TBAB (0.16 g, 0.5 mmol) and 2 M potassium carbonate aqueous solution (10 mL). We store the mixture at room temperature for 0.5 h under argon atmosphere. Then we add $Pd(PPh_3)_4$ (0.006 g, 9.0×10^{-3} mmol) to the mixture and heat to 90 ^{o}C for 24 h. After the mixture cools down to room temperature, we pour some water into the mixture and extract three times with ethyl acetate. We perform Na_2SO_4 to dry the combined organic solution and concentrate it in vacuums. We purify the crude with a silica gel column using n-hexane/CH_2Cl_2 as eluent to give TPE as yellow solid (1.71 g, yield: 95%). ^{1}H NMR (400 MHz, $CDCl_3$) δ ppm: 6.96-7.05 (m, 6 H), 7.07-7.15 (m, 9 H), 7.18 (d, 2 H, J = 8.1 Hz), 7.60 (d, 2 H, J = 8.7 Hz), 7.89 (s, 1 H).

1-methyl-2-(4-(1,2,2-triphenylvinyl)styryl)pyridinium iodide (TPE-Py) We dissolve TPE-CHO (210 mg, 0.58 mmol) and 1,2-dimethylpyridinium iodide (125 mg, 0.53 mmol) in ethanol (15 mL) and add a few drops of triethylamine. We reflux the mixture under nitrogen for 48 h. After the mixture cools down to room temperature, we remove the solvent under reduced pressure. We purify the residue with a silica gel column using CH_2Cl_2/MeOH (20:1 v/v) as eluent to produce a yellow solid (91 mg, yield: 30%). ^{1}H NMR

View Article Online
DOI: 10.1039/C7NR00342K

(400 MHz, $CDCl_3$) δ 9.32 (d, J = 5.3 Hz, 1H), 8.33 (t, J = 7.6 Hz, 1H), 8.25 (d, J = 8.0 Hz, 1H), 7.77 (t, J = 6.2 Hz, 1H), 7.58 (d, J = 15.8 Hz, 1H), 7.50 (d, J = 8.1 Hz, 2H), 7.35 (d, J = 15.9 Hz, 1H), 7.20 – 6.94 (m, 17H), 4.55 (s, 3H). ^{13}C NMR (101 MHz, $CDCl_3$) δ 153.22, 147.64, 146.69, 144.55, 143.23, 143.08, 142.65, 139.92, 132.14, 131.30, 128.36, 127.95, 127.72, 126.90, 125.53, 115.86, 47.42. HRMS (MALDI): [M^+] m/z calcd 450.2216, found 450.2213.

1-methyl-4-(4-(1,2,2-triphenylvinyl)styryl)quinolinium iodide (TPE-Quino) We add pyrrolidine (0.2 mL) dropwise to a solution of TPE-CHO (210 mg, 0.58 mmol) and 1,4-dimethylquinolinium iodide (151 mg, 0.53 mmol) in ethanol (15 mL). We stir the mixture at 30 ^{o}C for 24 h. We remove the solvent under reduced pressure and purify the residue with a silica gel column using CH_2Cl_2/MeOH (20:1 v/v) as the eluent to yield an orange solid (110 mg, yield: 53%). ^{1}H NMR (400 MHz, $CDCl_3$) δ 10.20 (d, J = 6.3 Hz, 1H), 8.54 (d, J = 8.4 Hz, 1H), 8.29 – 8.22 (m, 2H), 8.20 – 8.13 (m, 1H), 7.99 – 7.91 (m, 1H), 7.78 (d, J = 2.2 Hz, 2H), 7.49 (d, J = 8.3 Hz, 2H), 7.19 – 6.96 (m, 17H), 4.80 (s, 3H). ^{13}C NMR (101 MHz, $CDCl_3$) δ 153.41, 150.23, 147.56, 143.83, 143.30, 142.82, 140.07, 138.96, 135.20, 132.98, 132.36, 131.35, 129.43, 127.96, 126.96, 126.08, 118.53, 117.46, 45.13. HRMS (MALDI): [M^+] m/z calcd 500.2373, found 500.2359.

10-methyl-9-(4-(1,2,2-triphenylvinyl)styryl)acridinium iodide (TPE-Acr) We mix TPE-CHO (210 mg, 0.58 mmol) and 9,10-dimethylacridinium iodide (177 mg, 0.53 mmol) in dry ethanol and reflux the mixture under nitrogen atmosphere for 48 h. After the mixture cools to room temperature, we eliminate the solvent under reduced pressure. We purify the residue with a silica gel column using CH_2Cl_2/MeOH (20:1 v/v) as eluent to give a red solid (147 mg, yield: 40%).^{1}H NMR (400 MHz, $CDCl_3$) δ 8.84 (d, J = 9.2 Hz, 2H), 8.66 (d, J = 8.6 Hz, 2H), 8.44 – 8.35 (m, 2H), 8.05 (d, J = 16.3 Hz, 1H), 7.88 (dd, J = 8.4, 7.0 Hz, 2H), 7.51 (d, J = 8.3 Hz, 2H), 7.23 – 7.02 (m, 18H), 5.13 (s, 3H). ^{13}C NMR (101 MHz, $CDCl_3$) δ 157.94 , 147.11 , 146.43 , 143.37 , 142.67 , 141.46 , 140.03 , 138.95 , 132.98 , 132.39 , 131.37, 128.95 , 127.88 , 127.52 , 126.93 , 125.17, 119.60, 119.27.82. HRMS (MALDI): [M^+] m/z calcd 550.2529, found 550.2519.

Preparation of TPE-Py, TPE-Quino, and TPE-Acr organic nanoparticles

We prepare these nanoparticles by adding DMSO solutions of these compounds into phosphate buffered saline (PBS), and then vortex for ten minutes.

Cell culture

We culture the cells with Dulbecco's modified Eagle's medium (DMEM; Gibco) containing fetal bovine serum (FBS, 10%; Gibco), Penicillin&Streptomycin (1%), Glutamine (1%), and incubated in CO_2 (5%) at 37 ^{o}C.

The cytotoxicity of the TPE dots

We evaluate the cytotoxicity of TPE dots by Cell Counting Kit-8 (CCK-8). We seed human umbilical vein endothelial cells (HUVECs) at count 10000 cells/well on a 96 well plate and allow them to grow overnight. We expose the cells to different concentrations of TPE-Acr, TPE-Py, and TPE-Quino (1 μM, 2 μM, 3 μM, 4 μM, 5 μM, 6 μM, 7 μM, 8 μM) dots for 24 hours. After 24 hours, we wash the cells and stain them with CCK-8. A microplate reader (Tecan infinite M200) gives us the optical density of the cells at 450 nm after 2 hours of incubation at 37 ^{o}C.

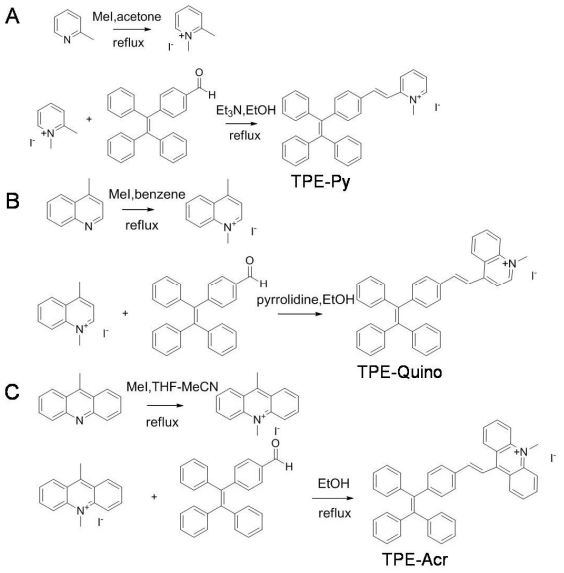

Scheme 1. Synthesis of TPE-Acr, TPE-Py, and TPE-Quino.

Microbe culture

We employ *Staphylococcus aureus* (*S. a*), *E. coli,* and *C. albicans* for this study. We pre-culture *S. a* and *E. coli* with Luria-Bertani (LB) broth at 37 ^{o}C to reach a concentration of about 10^{-7}CFUmL^{-1}. While *C. albicans* grow in potato dextrose agar (PDA) broth at 25 ^{o}C.

Cells and microbe imaging

We stain the live cells with TPE dots (5 μM) and MitoTracker Red (200 nM). We image the cells by using a confocal microscopy (Zeiss LSM710) and two-photon microscopy (OLYMPUS FV1000).

Results and discussion

Synthesis and characterization of the TPE derivatives

We prepare the fluorogens TPE-Py, TPE-Quino, and TPE-Acr following the synthetic route shown in Scheme 1 (see experimental section for detailed procedures). We characterize and confirm their structures via nuclear magnetic resonance (NMR) and high resolution mass spectrometry (HRMS). These analysis data correspond to their expected molecular structures. To further investigate the nano-aggregation, we characterize the morphology of aggregated TPE-Py, TPE-Quino, and TPE-Acr by transmission electron microscopy (TEM). These TPE molecules assemble into spherical nanoparticles with average sizes of 20-40 nm (Fig. 1C, 1D,

View Article Online
DOI: 10.1039/C7NR00342K

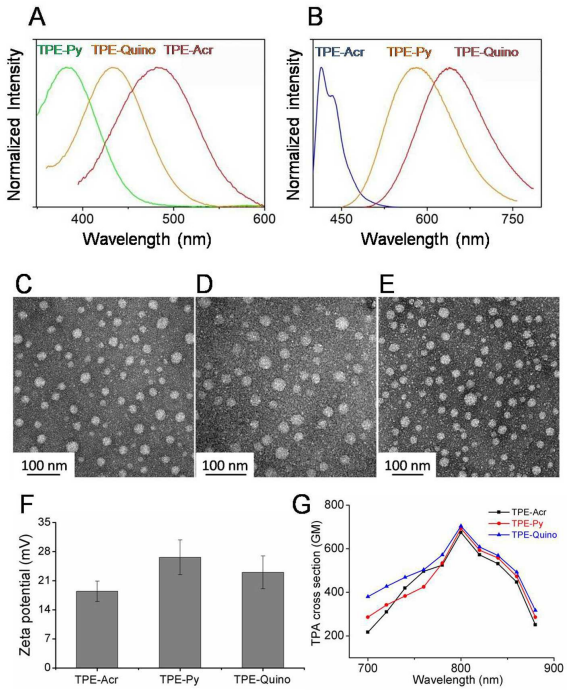

Fig. 1. Normalized spectrum and TEM images of the TPE nanodots. (A) UV spectrum of TPE-Acr, TPE-Py, and TPE-Quino in V_{PBST}:V_{DMSO}= 100:1. Solution concentration: 20 μM. (B) Emission spectrum of TPE-Acr, TPE-Py, and TPE-Quino. Excitation wavelength: 380 nm, 390 nm, and 405 nm, respectively. TEM images of the TPE nanodots: (C) TPE-Acr, (D) TPE-Py, and (E) TPE-Quino. (F) Zeta potential of TPE dots. (G) TPA cross section of TPE dots.

and 1E) which is corresponding to dynamic light scattering (DLS) analysis of particle sizes (Fig. S2B). We further test zeta potentials of these particles, these particles are positive charged (TPE-Acr: 18.45 ± 2.43 mV; TPE-Py: 26.62 ± 4.17 mV; TPE-Quino: 23.01 ± 3.94 mV). The difference of the zeta potentials is due to the imparity of π-system in the molecule structures (Fig. 1F). According to our system, when our molecule has big π bond, the corresponding particle have relative low charge. The aggregated AIE organic nanoparticles show fluorescence, and we call them AIE-dots. All of the TPE dots show superior fluorescence quantum yields (TPE-Acr: 0.64; TPE-Py: 0.53; TPE-Quino: 0.59) (Table S1). Researchers have reported the AIE-dots have two-proton fluorescence. However, the preparation of AIE-dots is inconvenient which needs polymers or cell-penetrating peptides to encapsulate the AIE molecules such that the dots can enter and stain cells and organs. [12] Our AIE-dots don't need the complex modification.

AIE-dots optical spectra in solutions

We explore the photophysical properties of the AIE-dots using ultraviolet (UV)-visible and fluorescence spectrophotometry. The dilute dimethylsulfoxide (DMSO) solution (20 μM) of TPE-Py exhibits a peak maximum of UV at 382 nm. The spectra of TPE-Quino and TPE-Acr locate at longer wavelength, 432 nm and 480 nm, revealing

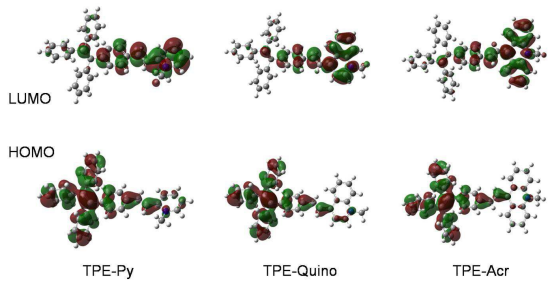

Fig. 2. LUMO and HOMO distribution of TPE-Py, TPE-Quino, and TPE-Acr.

that they possess better conjugation than TPE-Py (Fig. 1A). We also measure the fluorescence properties of these AIE-dots. We present the emission intensities of TPE compounds in different reagents (Fig. S1). We find that the dilute tetrahydrofuran (THF) solutions of TPE-Acr, TPE-Py, and TPE-Quino have weak emission. Phosphate-buffered saline with 0.1% Tween 20 (PBST) solutions of TPE-Acr, TPE-Py, and TPE-Quino have larger emission intensities than other solvents due to aggregation. We thus use PBST to induce the aggregation from THF. When we add PBST to the THF solutions of TPE-Acr, TPE-Py, and TPE-Quino, the emissions have no marked variations. But the emissions markedly increase when the fraction of PBST are over 70%. The fluorescence of three kinds of AIE dots has ranged different colors with large stokes shifts which cover a large portion of the visible spectrum (Fig. 1B).

In order to further investigate the two-photon ability of TPE dots, we measure their two-photon absorption (TPA) cross-sections (δ) in the wavelength range from 700-880 nm (Fig. 1G). The maximum δ is 675 GM at 800 nm for TPE-Acr, 693 GM at 800 nm for TPE-Py, and 704 GM at 800 nm for TPE-Quino. Notably, these dots show similar and high TPA cross-sections (over 100 GM). Such results indicate that small extended π-system can hardly enhance the two-photon cross-section of the dye in our system. We also compare one-photon excited fluorescence (OPEF) spectra with two-photon excited fluorescence (TPEF) spectra of TPE-Acr, TPE-Py, and TPE-Quino (Fig. S2A). The TPEF spectra resemble the OPEF spectra except for a slight red-shift, due to different spectral selection rules.

To gain insight into intramolecular charge-transfer (ICT) from TPE core to N-containing heterocycles, we calculate their electronic structures using the density functional theory (DFT) method based on the Gaussian 09 programs. The highest occupied molecular orbitals (HOMO) of TPE-Py, TPE-Quino, and TPE-Acr mainly locate in TPE moieties. Like the HOMO, N-containing heterocycles moieties dominate the lowest unoccupied molecular orbitals (LUMO) of TPE-Py, TPE-Quino, and TPE-Acr (Fig. 2). Density changes of the electron clouds of these probes manifest unambiguous ICT from TPE moiety (donor) to N-containing heterocycles groups (acceptor). These results are well consistent with D-π-A molecular geometry what we designed.

Bioimaging with one-photon excitation

View Article Online
DOI: 10.1039/C7NR00342K

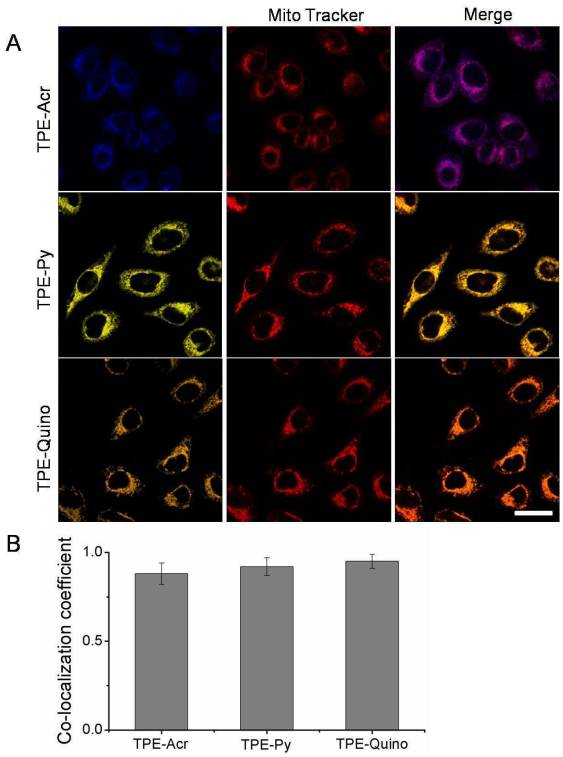

Fig. 3. One-photon abilities of these AIE dots: (A) HeLa cells images using TPE-dots (5 μM); Mitochondrial images with Mito Tracker Red (200 μM); and merged images. Scale bar: 30 nm. (B) co-localization coefficient of the photos in (A).

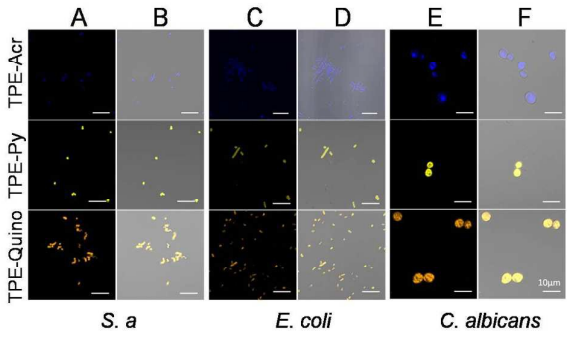

Fig. 4. One-photon ability: Microbes images using TPE-dots. (A) *S. a,* (C) *E. coli,* and (E) *C. albicans* images using TPE-dots (5 μM). (B) *S. a*, (D) *E. coli,* and (F) *C. albicans* merged images of AIE-dots and cell morphology (bright fields).

We assess TPE-Acr, TPE-Py, and TPE-Quino for their ability to stain living cells. HeLa cells grow overnight on confocal culture dishes. We add 5 μM of each TPE dots which contain the essential medium to dilute them completely to form dots to cells. After incubation for

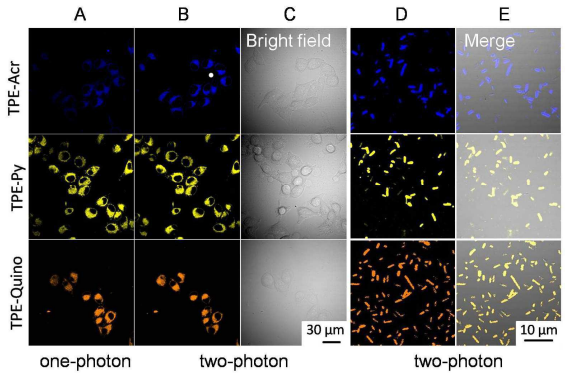

Fig. 5. Two-photon abilities of AIE-dots. (A) one-photon and (B) two-photon excited images in the same location. (C) Bright field image of HeLa cells. (D) Two-photon images of *E. coli* and (E) Merged pictures with bright field of *E. coli*.

20 min at 37 °C maintained in 5% CO_2, we image the cells directly on a confocal microscope (Zesis LSM710) without washing them. The TPE dots stain almost all of the HeLa cells (Fig. 3 and S3). Interestingly, we find strong emissions generated from mitochondria regions of living cells when we use 405 nm excitation light supplied by a confocal microscope. In order to verify this observation, we use MitoTracker Red FM, a far red-fluorescent mitochondria staining dye, to co-stain HeLa cells with TPE dyes. The co-staining experiments show outstanding overlaps in the merged photos, suggesting that TPE-Acr, TPE-Py, and TPE-Quino can image the mitochondria of living cells specifically. Pearson's colocalization coefficient which is collected from the photos also confirms that the TPE dots can target mitochondria accurately (Fig. 3B). Compared with the commercially available mitochondrial dyes, these TPE dots do not require washing due to their AIE feather and low cytotoxicity (Fig. S4). These dyes without the washing step make the staining process more convenient and economical. Furthermore, we also employ these TPE dots to stain HUVECs and NIH 3T3 cells (Fig S5). As expected, the dyes can target these kinds of cells which indicate these TPE derivatives are useful for imaging mitochondria.

We explore the application of these TPE compounds as fluorescent agents in microbial imaging. We utilize *S. a*, *E. coli,* and *C. albicans* for this study. We pre-culture *S. a* and *E. coli* with LB broth at 37 °C to reach a concentration of about 10^{-7} colony forming units per mL (CFU mL^{-1}). While *C. albicans* are grown in PDA broth at 25 °C. We use 5 μM TPE dyes to stain the prepared microbes respectively for about 20 minutes. Then we place a 10 μL microbe suspensions onto confocal microscopy slides and observe them using a confocal microscope. The nano dots can image gram-positive bacteria (*S. a*), gram-negative bacteria (*E. coli*), and fungus (*C. albicans*) with different fluorescence (Fig 4A, 4C, and 4E). Moreover, These AIE dots can target the microbes effectively (Fig 4B, 4D, and 4F). Evidently, these dots show excellent bioimaging activity for different kinds of cells and microbes with one-photon excitation.

Bioimaging with two-photon excitation

View Article Online
DOI: 10.1039/C7NR00342K

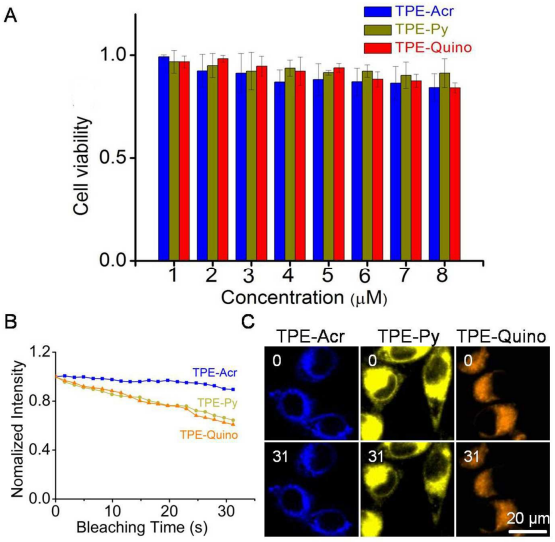

Fig. 6. Cytotoxicity and photostability of these AIE-dots. (A) Viability of HeLa cells after incubation with TPE nano-suspensions at different dyes concentrations for 24 h; (B) Signal loss of fluorescence emission with increasing time of bleaching using two-photon excitation and (C) Fluorescence images of HeLa cells stained with TPE-Acr, TPE-Py, and TPE-Quino dots at 0 and 31 bleaching time respectively.

Compared to conventional one-photon confocal laser scanning microscope, the two-photon microscope exhibits numbers of advantages, such as reduced substrate autofluorescence and self-absorption, and deeper tissue penetration[34]. In view of this, to evaluate the effect of these probes in living cells with their two-photon property, as our design, we use two-photon fluorescence microscopy to image cells incubated with these AIE-dots. We perform the assay with HeLa cells in the same way as single photon image. We obtain the images with excitation at 780 nm with 420-460 nm (TPE-Acr), 520-560 nm (TPE-Py), and 575-630 nm (TPE-Quino) bandpass filters respectively. We can observe blue, yellow, and orange signals clearly from HeLa cells (Fig. 5B). To show one-photon and two-photon abilities of AIE dots more intuitively, we also image the same location of cells using one-photon excitation (Fig. 5A).To our delight, all of these probes can stain living cells with the two-photon behavior.

We also explore two-photon property of the AIE-dots in the field of microbes. We choose *E. coli* as the example to investigate two-photon imaging of microbes. The preparation of two-photon *E. coli* samples is the same as one-photon *E. coli* samples. These AIE dots can label *E. coli* successfully and thus they will be particularly valuable in various bioimaging tasks (Fig. 5D and 5E).

These results indicate that AIE dots can serve as a promising one-photon and two-photon fluorescent probes for various biological samples.

Cytotoxicity and photostability of these AIE-dots

As sensors for live organisms, low cytotoxicity and good biocompatibility to target biosubstrates are of high importance. We evaluate the cytotoxicity of TPE-Acr, TPE-Py, and TPE-Quino dots using cell counting kit-8 (CCK-8) and cervical cancer HeLa cells. The cell viabilities remain acceptable under the experimental conditions which are in accordance with the cell morphologies in brightfield mode (Fig 6A and 5C). These AIE dots are of good biocompatibility for bioimaging applications.

To further investigate the abilities of AIE dots as ideal dyes, we characterize their photostabilities by continuous laser irradiation. In order to collect the real-time images, we apply the laser of the two-photon microscopy with excitation of 780 nm and transmissivity of 8.1%. The fluorescence intensity of TPE-Acr almost does not decay, while the signal loss of TPE-Py and TPE-Quino is about 40% after laser irradiation (Fig 6B). However, from the images of the stained cells (Fig 6C), we can see that the photobleaching of these dyes are acceptable in view of the high transmissivity of microscopy we used.

Conclusions

In this work, we develop a series of sensors for targeting mitochondria and microbes based on luminescent nanomaterials, which consist of TPE peripheries and N-heterocycles and are excited by one- or two-photon excitation. We reveal that their photostability and cytotoxicity are suitable for bioimaging. Our sensors have no need to wash them when we image cells and microbes, which is more suitable and convenient than other probes. We believe that organic AIE dots with tunable fluorescence wavelengths are promising biosensors to investigate the behaviors of cells and microbes with two kinds of excited modes which can fundamentally broaden the application of the probes in bioimaging field.

Acknowledgements

We thank the Ministry of Science and Technology of China (2013YQ190467), Chinese Academy of Sciences (XDA09030305) and the National Science Foundation of China (81361140345, 51373043, 21535001) for financial support.

Notes and references

1. M. R. Duchen, *Mol. Aspects Med.*, 2004, 25, 365-451.
2. M. T. Lin and M. F. Beal, *Nature*, 2006, 443, 787-795.
3. J. I. Hayashi, S. Ohta, A. Kikuchi, M. Takemitsu, Y. Goto and I. Nonaka, *Proc. Natl. Acad. U. S. A.*, 1991, 88, 10614-10618.
4. P. M. Abou-Sleiman, M. M. K. Muqit and N. W. Wood, *Nat. Rev. Neurosci.*, 2006, 7, 207-219.
5. H. B. Xiao, P. Li, W. Zhang and B. Tang, *Chem. Sci.*, 2016, 7, 1588-1593.
6. Q. F. Zhuang, H. Y. Jia, L. B. Du, Y. C. Li, Z. Chen, S. P. Huang and Y. Liu, *Biosens. Bioelectron.*, 2014, 55, 76-82.
7. G. Feng, D. Ding and B. Liu, *Nanoscale*, 2012, 4, 6150-6165.

View Article Online
DOI: 10.1039/C7NR00342K

8. S. Zhu, Q. Meng, L. Wang, J. Zhang, Y. Song, H. Jin, K. Zhang, H. Sun, H. Wang and B. Yang, *Angew. Chem. Int. Ed.*, 2013, 52, 3953-3957.
9. F. Miao, W. J. Zhang, Y. M. Sun, R. Y. Zhang, Y. Liu, F. Q. Guo, G. F. Song, M. G. Tian and X. Q. Yu, *Biosens. Bioelectron.*, 2014, 55, 423-429.
10. S. Liu, L. Wang, Y. L. Luo, J. Q. Tian, H. L. Li and X. P. Sun, *Nanoscale*, 2011, 3, 967-969.
11. X. Xue, Y. Zhao, L. Dai, X. Zhang, X. Hao, C. Zhang, S. Huo, J. Liu, C. Liu, A. Kumar, W. Q. Chen, G. Zou and X. J. Liang, *Adv. Mater.*, 2014, 26, 712-717.
12. D. Wang, J. Qian, W. Qin, A. Qin, B. Z. Tang and S. He, *Sci. Rep.*, 2014, 4, 4279-4287.
13. X. G. Gu, E. G. Zhao, T. Zhao, M. M. Kang, C. Gui, J. W. Y. Lam, S. W. Du, M. M. T. Loy and B. Z. Tang, *Adv. Mater.*, 2016, 28, 5064-5071.
14. Y. Y. Yuan, C. J. Zhang and B. Liu, *Angew. Chem. Int. Ed.*, 2015, 54, 11419-11423.
15. C. W. Leung, Y. Hong, S. Chen, E. Zhao, J. W. Lam and B. Z. Tang, *J. Am. Chem. Soc.*, 2013, 135, 62-65.
16. L. Zhang, W. W. Liu, X. H. Huang, G. X. Zhang, X. F. Wang, Z. Wang, D. Q. Zhang and X. Y. Jiang, *Analyst*, 2015, 140, 5849-5854.
17. W. E. Walden, *Proc. Natl. Acad. U. S. A.*, 2002, 99, 4138-4140.
18. V. Petronilli, I. Szabo and M. Zoratti, *FEBS Lett.*, 1989, 259, 137-143.
19. H. Chang, A. Ikram, F. Kosari, G. Vasmatzis, A. Bhunia and R. Bashir, *J. Vac. Sci. Technol. B*, 2002, 20, 2058-2064.
20. D. A. Rasko and V. Sperandio, *Nat. Rev. Drug Discov.*, 2010, 9, 117-128.
21. T. J. Rogers and E. Balish, *Microbiol. Rev.*, 1980, 44, 660-682.
22. P. Wang, Y. Y. Zhao, Y. Tian and X. Y. Jiang, *Nanomed.Nanotechnol.*, 2016, 12, 527-528.
23. Y. Y. Zhao, Y. Tian, Y. Cui, W. W. Liu, W. S. Ma and X. Y. Jiang, *J. Am. Chem. Soc.*, 2010, 132, 12349-12356.
24. Y. Y. Zhao, C. J. Ye, W. W. Liu, R. Chen and X. Y. Jiang, *Angew. Chem. Int. Ed.*, 2014, 53, 8127-8131.
25. Y. Y. Zhao, Z. L. Chen, Y. F. Chen, J. Xu, J. H. Li and X. Y. Jiang, *J. Am. Chem. Soc.*, 2013, 135, 12940-12943.
26. W. Chen, Q. Li, W. Zheng, F. Hu, G. Zhang, Z. Wang, D. Zhang and X. Jiang, *Angew. Chem. Int. Ed.*, 2014, 53, 13734-13739.
27. Y. Liu, Z. Wang, G. Zhang, W. Zhang, D. Zhang and X. Jiang, *Analyst*, 2012, 137, 4654-4657.
28. H. M. Kim and B. R. Cho, *Chem. Rev.*, 2015, 115, 5014-5055.
29. S. J. K. Pond, M. Rumi, M. D. Levin, T. C. Parker, D. Beljonne, M. W. Day, J. L. Bredas, S. R. Marder and J. W. Perry, *J. Phys. Chem. A*, 2002, 106, 11470-11480.
30. X. R. Shi, Z. Z. Xu, Q. Liao, Y. S. Wu, Z. J. Gu, R. H. Zheng and H. B. Fu, *Dyes Pigments*, 2015, 115, 211-217.
31. K. P. Divya, S. Sreejith, P. Ashokkumar, K. Yuzhan, Q. W. Peng, S. K. Maji, Y. Tong, H. Yu, Y. L. Zhao, P. Ramamurthy and A. Ajayaghosh, *Chem. Sci.*, 2014, 5, 3469-3474.
32. Q. Q. Li, J. Huang, A. S. Zhong, C. Zhong, M. Peng, J. Liu, Z. G. Pei, Z. L. Huang, J. G. Qin and Z. Li, *J. Phys. Chem. B*, 2011, 115, 4279-4285.
33. D. Ding, C. C. Goh, G. Feng, Z. Zhao, J. Liu, R. Liu, N. Tomczak, J. Geng, B. Z. Tang, L. G. Ng and B. Liu, *Adv. Mater.*, 2013, 25, 6083-6088.
34. W. Zhang, J. Kang, P. Li, L. Liu, H. Wang and B. Tang, *Chem. Commun.*, 2016, 52, 13991-13994.
35. J. B. Shi, Y. M. Wu, S. Sun, B. Tong, J. G. Zhi and Y. P. Dong, *J. Polym. Sci. Pol. Chem.*, 2013, 51, 229-240.
36. M. Kervinen, J. Patsi, M. Finel and I. E. Hassinen, *Anal. Biochem.*, 2004, 324, 45-51.
37. A. S. Waggoner, *Annu. Rev. Biophys. Bio.*, 1979, 8, 47-68.
38. J. S. Dickson and M. Koohmaraie, *Appl. Environ. Microb.*, 1989, 55, 832-836.
39. S. Chalmers, S. T. Caldwell, C. Quin, T. A. Prime, A. M. James, A. G. Cairns, M. P. Murphy, J. G. McCarron and R. C. Hartley, *J. Am. Chem. Soc.*, 2012, 134, 758-761.
40. Z. J. Zhao, P. Lu, J. W. Y. Lam, Z. M. Wang, C. Y. K. Chan, H. H. Y. Sung, I. D. Williams, Y. G. Ma and B. Z. Tang, *Chem. Sci.*, 2011, 2, 672-675.
41. N. Zhao, M. Li, Y. L. Yan, J. W. Y. Lam, Y. L. Zhang, Y. S. Zhao, K. S. Wong and B. Z. Tang, *J. Mater. Chem. C*, 2013, 1, 4640-4646.
42. S. Wroblewski, K. Trzebiatowska, B. Jedrzejewska, M. Pietrzak, R. Gawinecki and J. Paczkowski, *J. Chem. Soc. Perk. Trans. 2*, 1999, 2, 1909-1917.
43. H. Suzuki and Y. Tanaka, *J. Org. Chem.*, 2001, 66, 2227-2231.

View Article Online
DOI: 10.1039/C7NR00342K

Graphical abstract

We develop a series of sensors for targeting mitochondria and microbes based on luminescent nanomaterials, which consist of TPE peripheries and N-heterocycles and are excited by one- or two-photon excitation.